SOME PRESENT LIMITATIONS ON THE LATTICE IMAGING OF GRAIN BOUNDARIES

W. Mader, G. Necker, R. Balluffi

JOURNAL DE PHYSIQUE
Colloque C5, supplément au n°10, Tome 49, octobre 1988

SOME PRESENT LIMITATIONS ON THE LATTICE IMAGING OF GRAIN BOUNDARIES

W. MADER, G. NECKER and R.W. BALLUFFI*

Max-Planck-Institut für Metallforschung, Institut für Werkstoffwissenschaften, Seestrasse 92, D-7000 Stuttgart 1, F.R.G.
**Department of Materials Science and Engineering, Massachusetts Institute of Technology, Cambridge, MA 02139, U.S.A.*

Abstract - Limitations which currently exist on using the electron microscope lattice imaging technique to obtain information about grain boundary structure are considered. Boundaries are only amenable when the adjoining crystals are oriented so that they produce projected patterns of resolved atomic columns or atomic planes. The conditions under which information can then be obtained about the atomistic core structure, the boundary translational state and the presence of localized grain boundary dislocations are described. In a number of instances, ultra-thin bicrystals are required which are so thin that great difficulties will be encountered with utilizing them on a practical basis.

1. Introduction - In the present paper, we discuss the limitations which currently exist on using the electron microscope lattice imaging technique to obtain information about the structure of grain boundaries. In this technique, attempts are made to obtain projected images of the boundary structures. The general arrangement is illustrated in Fig. 1, where the boundary lies in a plate-shaped bicrystal specimen, and the plane of projection is perpendicular to $\underline{e}$, the direction of the electron beam. The vector $\underline{s}$ is normal to the specimen surface, the vector $\underline{n}$ is normal to the grain boundary, and $\underline{e}$, $\underline{s}$ and $\underline{n}$ are generally non-coplanar. In almost all previous lattice imaging studies (1-3), a geometry with $\underline{s} \parallel \underline{e}$ and $\underline{n} \perp \underline{e}$ has been used for studies of tilt boundaries. In this particular case, the images of crystals 1 and 2 appear side by side separated by the image of the grain boundary region which is viewed edge-on along the tilt axis. The core region along the beam direction is therefore relatively long (equal to the crystal thickness) and the projection of its atomistic structure can often be imaged. In addition, information about the grain boundary translational state (i.e., the specification of the translation position of Crystal 2 with respect to Crystal 1) in the plane of projection can be obtained. Recently, the authors (4) have examined a second special case with $\underline{s} \parallel \underline{n} \parallel \underline{e}$. In this case, the boundary was a twist boundary viewed at normal incidence, and the projections of Crystals 1 and 2 and the core region were all superimposed. Since the boundary core region was extremely thin along the beam direction, its contribution to the overall image obtained from the bicrystal was undetectable. Nevertheless, we found that information about the grain boundary translational state in the plane of projection could still be obtained from an analysis of the observed pattern produced by Crystals 1 and 2. In addition, the presence of arrays of localized screw grain boundary dislocations could be detected when the specimen was thinner than the dislocation spacing.

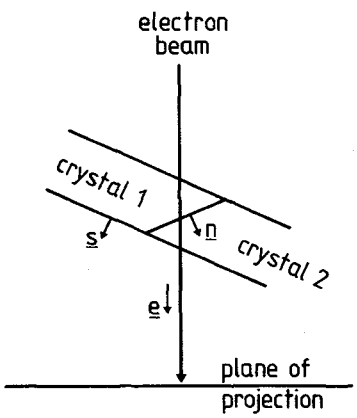

Fig. 1. General specimen arrangement for grain boundary lattice imaging.

In the following, we discuss more generally the present limitations on the use of lattice imaging for the study of grain boundaries. Of particular interest is the range of boundary types in FCC metals which can be studied with the best electron microscopes available at present and the types of information which can be obtained.

2. Basic Conditions for Imaging - In order to obtain any type of useful image, it is necessary, of course, for both Crystals 1 and 2 to be oriented so that they produce projected patterns of either atomic columns (which appear as an array of spots) or atomic planes (which appear as an array of parallel lines) which are reasonably well resolved. With the present limit of resolution (information resolution limit ≃ 0.14 nm) of the electron microscopes available, this can only be done for most FCC crystals oriented with respect to the electron beam to create the point and line patterns shown in Fig. 2. We note that the number of (resolvable) orientations is somewhat more restricted in the case of FCC metals with relatively small lattice constants, such as Cu and Ni. Therefore, only boundaries with the two adjoining grains corresponding to these orientations are currently amenable.

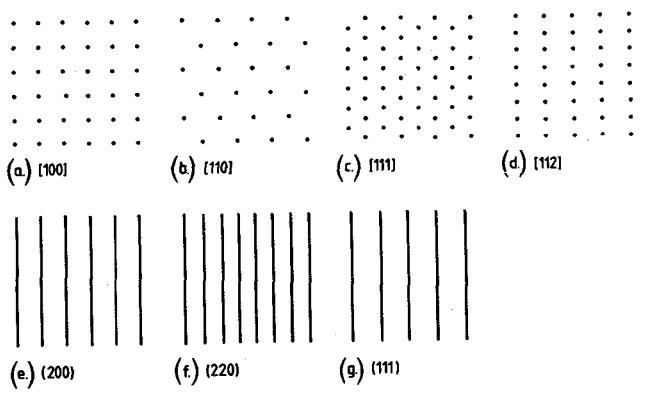

Fig. 2. Projected point and line patterns resolvable for FCC crystals with current microscopes. (a)-(d) are formed by atomic columns viewed along [hkl]. (e)-(g) are formed by (hkl) atomic planes viewed edge-on along any direction ⊥ [hkl].

A principal limitation on resolving individual atomic columns or atomic planes is given by the extensive atomic scattering potentials for the electrons. The scattering potentials of closely spaced ($d \leq 0.05$ nm) atomic columns overlap and, hence, cannot be imaged separately by any electron microscope. Also, we note that the superposition of scattering potentials increases with increasing temperature (thermal vibrations) and with the atomic number.

3. Information about the Atomistic Core Structure - Two main cases can be distinguished:

(i) $\underline{e} \perp \underline{n}$: the projections of the two crystals appear side by side separated by the boundary core which is viewed edge-on, and, hence, is long in the beam direction. If the conditions in Section 2 are fulfilled, at least some information should then be obtained about the core structure of many types of boundaries. Notice that such boundaries include many which are not tilt boundaries. The most amenable boundaries, of course, are those tilt boundaries where the atomic columns are resolved on both sides of the boundary and where the core structure possesses a relatively short period, both along $\underline{e}$ and perpendicular to it. No particular imaging difficulties should occur when $\underline{s} \perp \underline{e}\underline{x}\underline{n}$. However, when $\underline{s}$ possesses an appreciable component along $\underline{e}\underline{x}\underline{n}$, different parts of the boundary core will be imaged under different focusing conditions. However, this gradual change of focus (contrast) should be much less severe than, for example, image contrast variations due to thickness variations of the foil.

(ii) $\underline{e}$ not $\perp \underline{n}$: the image of the projected grain boundary region is superimposed on the images of Crystals 1 and 2. Since the grain boundary thickness is very small, any effects due to the scattering from the core region will be correspondingly small. In fact, as we show below, because of this it seems likely that no information about the core structure can be obtained with this geometry under normally attainable experimental conditions.

In order to evaluate the contribution of the core structure in Case (ii) above, we have calculated images of gold bicrystals containing [001] Σ5 (θ=36.9°) twist boundaries with different assumed core structures for the case $\underline{e} \parallel \underline{n} \parallel \underline{s}$. In each case, the CSL translational state parallel to the boundary was maintained. In the first case (Model A), a rigid bicrystal was assumed and no relaxation was allowed in the first planes of Crystals 1 and 2 facing the boundary midplane (Fig. 3a). In the second case (Model B), the atoms in the first planes facing the boundary midplane were relaxed to the configuration shown in Fig. 3b in the manner described in (5). In the third case (Model C), an additional plane of atoms with the configuration shown in Fig. 3c was inserted in the boundary midplane between the rigid Crystals 1 and 2 illustrated in Fig. 1a. In the fourth case (Model D), a gap in the boundary was created by starting with the configuration in Fig. 3a and then rigidly displacing Crystal 1 with respect to Crystal 2 a distance 0.2 nm along [001].

The image calculations were carried out for bicrystal thicknesses between 1 nm - 10 nm (the grain boundary was always kept in the midplane of the bicrystal) using the multislice method (program package EMS (6)) where each (002) plane was taken as a phase grating for the electron waves. The calculations assumed a 200 kV microscope having an objective lens with spherical aberration coefficient C_S=1 mm and focusing distance f=94 nm (second broad phase contrast zone leading to contrast reversal) where details appeared most distinct in the images.

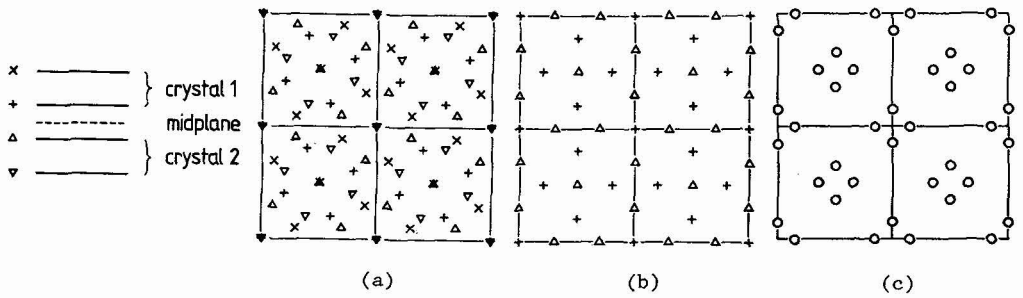

Fig. 3. (a) [001] projection of rigid bicrystal containing a [001] Σ5 twist boundary in the unrelaxed CSL translational state (4) corresponding to the Model A configuration (see text). The stacking sequence of the (001) planes is shown in the side view on the left. (b) Projected view of first planes in Crystals 1 and 2 facing the boundary midplane in the Model B configuration (see text). (c) Projected view of additional plane inserted in the boundary midplane in the Model C configuration (see text).

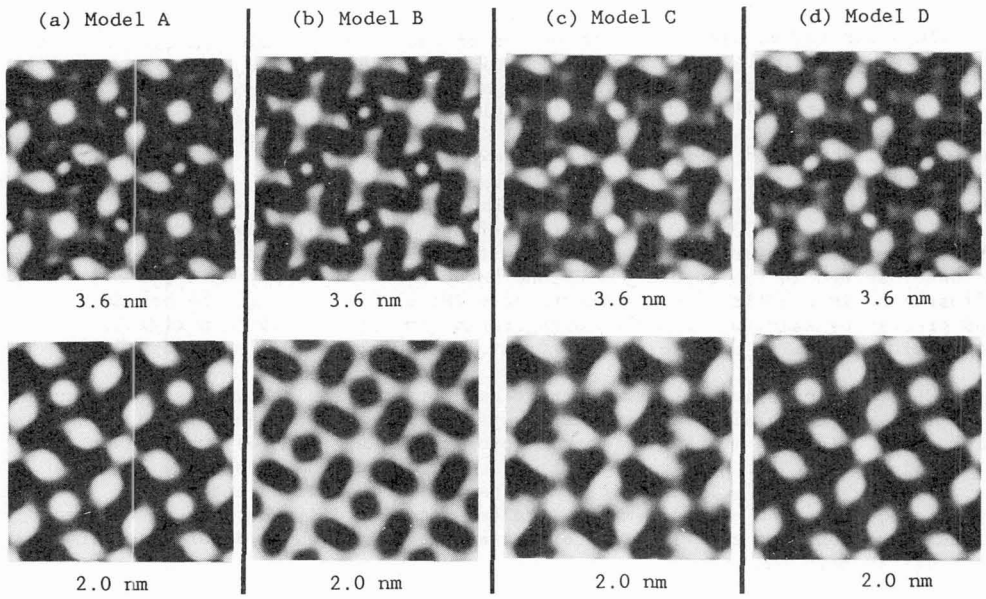

Fig. 4.. Calculated lattice images of Au bicrystals, 3.6 and 2.0 nm thick, containing [001] $\Sigma 5$ twist boundaries corresponding to Models A, B, C, and D described in text. Each image corresponds to the 4 projected cells illustrated in Fig. 3.

The calculations for Models A and D showed that the projected image was unaffected by the introduction of the gap in the boundary for all bicrystal thicknesses as might have been expected. A comparison of Figs. 4a and 4d demonstrates this result for thicknesses of 3.6 and 2.0 nm. Also, all images for Models A, B, and C were identical for bicrystal thicknesses >5 nm. For these relatively thick specimens, the scattering from the various thin core regions was clearly too small to have produced any noticeable effect. However, noticeable differences developed for very thin bicrystals with thicknesses in the range ≤ 4 nm. This result for Models A, B, and C is illustrated in Figs. 4a, b, and c where images are shown for bicrystal thicknesses again equal to 3.6 and 2.0 nm. Only small differences are seen for the 3.6 nm thick bicrystals but larger ones appear for the 2.0 nm thick bicrystals, particularly for the Model B boundary. These results clearly demonstrate that more and more information is revealed about the core structures as the bicrystal thickness is progressively reduced below ~4 nm. However, it must be stressed that it will be exceedingly difficult to prepare and handle bicrystal specimens with thicknesses as small as the 2.0 nm (or smaller) values that might be required. (In such cases, each crystal is only some 5 atomic planes thick!) We have found that the grain structures of layered bicrystal specimens of the type considered here are only marginally metastable and that 10 nm thick bicrystals often quickly convert to more stable columnar structures even under very moderate electron microscope beam heating. In addition, with decreasing foil thicknesses, lattice images are increasingly influenced by surface contamination or surface structure (surface reconstruction) so that the image interpretation becomes very complicated.

4. Information about the Translational State of the Boundary - Since only relative translations of the projected patterns of Crystals 1 and 2 can be observed, all information about the boundary translational state is restricted to the plane of projection. In general, distinguishable translational states for a grain boundary will occur only when the DSC-Lattice (DSCL) produced by Crystals 1 and 2 is reasonably coarse. (This is a result of the fact that all possible translational states fall within the primitive cell of the DSCL.) We have therefore investigated the DSCLs produced by the various possible pairs of projected FCC crystal patterns, shown in Fig. 2, and the results are shown

in the Table. Briefly, when the bicrystal projection consists of two point patterns with $[uvw]_1 = [uvw]_2$ relatively coarse 2-D DSCLs are formed when the point patterns are misoriented to produce the relatively small CSLs corresponding to the Σ values indicated. In such cases, both components of the translational state in the plane of projection can be measured. When the CSL becomes very large and the DSCL becomes correspondingly fine, all possible translational states become indistinguishable. In other cases, only 1-D DSCLs are formed. In such cases, the only component of the translational state which is physically distinguishable is parallel to the DSCL. When no appreciably coarse DSCL is formed, the two lattices are essentially incommensurate, and all translational states are physically indistinguishable.

5. Information about Localized Grain Boundary Dislocation (GBD) Structures - In our previous work (4), we demonstrated that arrays of localized GBDs can be detected by lattice imaging at normal incidence to the boundary ($\underline{e} \parallel \underline{n}$) when the specimen thickness is smaller than the GBD spacing so that the GBD strain field extends through the specimen thickness. It is also well established that GBDs can be detected in boundaries observed edge-on when they run parallel to $\underline{e}$. It is clear therefore that it should be possible to detect localized GBDs under a wide range of conditions if sufficiently thin specimens are employed.

6. Summary and Conclusions

(i) Lattice imaging studies of grain boundaries are presently restricted to a limited number of grain boundary types for which the adjoining crystals are mutually oriented to produce resolvable point or line patterns. Various types of structural information can be obtained for these boundaries under different conditions.

(ii) Information about the atomistic core structure can be obtained for a variety of boundaries (including mixed boundaries) under a wide range of imaging conditions and specimen geometries when $\underline{e} \perp \underline{n}$ (Fig. 1). Comparable

information cannot be obtained with $\underline{e}$ not $\perp$ $\underline{n}$ unless the specimen is sufficiently thin. However, sufficiently thin specimens will be extremely difficult to prepare and utilize under practical conditions.
(iii) Information about the boundary translational state in the plane of projection can be obtained with $\underline{e} \perp \underline{n}$ and also $\underline{e}$ not $\perp$ $\underline{n}$.
(iv) Information about the presence of arrays of localized grain boundary dislocations (GBDs) can be obtained with both $\underline{e} \perp \underline{n}$ and $\underline{e}$ not $\perp$ $\underline{n}$. However, in the latter case, the specimen must be thin enough so that the GBD strain field extends through the specimen thickness.

Table. List of relatively coarse DSC-Lattices (DSCLs) produced by the projected patterns of atomic columns or planes illustrated in Fig. 2.

Boundary	Projected Pattern (See Fig. 2)	DSCLs Formed	d/a*
1	$[100]_1$ on $[100]_2$	2-D DSCLs when Σ = 5,13 . .	1/2√5**
2	$[110]_1$ on $[110]_2$	2-D DSCLs when Σ = 3, 9 . .	1/√24**
3	$[111]_1$ on $[111]_2$	2-D DSCLs when Σ = 7,13 . .	1/√42**
4	$[112]_1$ on $[112]_2$	2-D DSCLs when Σ = 5, 7 . .	1/√30**
5	$[100]_1$ on $[110]_2$	1-D DSCL when $\langle 100\rangle_1 \parallel \langle 100\rangle_2$	1/2
		1-D DSCL when $\langle 110\rangle_1 \parallel \langle 110\rangle_2$	1/√2
6	$[100]_1$ on $[111]_2$	1-D DSCL when $\langle 110\rangle_1 \parallel \langle 110\rangle_2$	1/√2
7	$[100]_1$ on $[112]_2$	1-D DSCL when $\langle 110\rangle_1 \parallel \langle 110\rangle_2$	1/√8
8	$[110]_1$ on $[111]_2$	1-D DSCL when $\langle 110\rangle_1 \parallel \langle 110\rangle_2$	1/√2
		1-D DSCL when $\langle 112\rangle_1 \parallel \langle 112\rangle_2$	1/√24
9	$[110]_1$ on $[112]_2$	1-D DSCL when $\langle 110\rangle_1 \parallel \langle 110\rangle_2$	1/√8
10	$[111]_1$ on $[112]_2$	1-D DSCL when $\langle 110\rangle_1 \parallel \langle 110\rangle_2$	1/√8
11	$[100]_1$ on $(200)_2$	1-D DSCL when $\langle 100\rangle_1 \parallel \langle 100\rangle_2$	1/2
		1-D DSCL when $\langle 430\rangle_1 \parallel \langle 100\rangle_2$	1/10
12	$[110]_1$ on $(200)_2$	1-D DSCL when $\langle 100\rangle_1 \parallel \langle 100\rangle_2$	1/2
13	$[111]_1$ on $(200)_2$		
14	$[112]_1$ on $(200)_2$		
15	$[100]_1$ on $(220)_2$	1-D DSCL when $\langle 110\rangle_1 \parallel \langle 110\rangle_2$	1/√8
16	$[110]_1$ on $(220)_2$	1-D DSCL when $\langle 110\rangle_1 \parallel \langle 110\rangle_2$	1/√8
		1-D DSCL when $\langle 114\rangle_1 \parallel \langle 110\rangle_2$	1/6√2
17	$[111]_1$ on $(220)_2$	1-D DSCL when $\langle 110\rangle_1 \parallel \langle 110\rangle_2$	1/√8
18	$[112]_1$ on $(220)_2$	1-D DSCL when $\langle 110\rangle_1 \parallel \langle 110\rangle_2$	1/√8
19	$[100]_1$ on $(111)_2$		
20	$[110]_1$ on $(111)_2$	1-D DSCL when $\langle 111\rangle_1 \parallel \langle 111\rangle_2$	1/√3
21	$[111]_1$ on $(111)_2$		
22	$[112]_1$ on $(111)_2$	1-D DSCL when $\langle 111\rangle_1 \parallel \langle 111\rangle_2$	1/√3

*d = DSCL spacing; a = lattice parameter.
**Only coarsest spacing of the DSCL corresponding to the smallest Σ which is listed is given.

Acknowledgement - RWB thanks the Alexander von Humboldt Foundation for a Senior Scientist Award and the U.S. Department of Energy for additional support under Grant No. DE-FG02-84ER45116.

References

(1) Gronsky, R. in Grain Boundary Structure and Properties, ed. R. W. Balluffi, American Soc. for Metals, Metals Park, Ohio (1980) 45.
(2) D'Anterroches, C., and Bourret, A., Phil. Mag. A 49 (1984) 783.
(3) Krakow, W. and Smith, D. A., Ultramicroscopy 22 (1987) 47.
(4) Mader, W., Necker, G., Babcock, S. E. and Balluffi, R. W., Scripta Metall. 21 (1987) 555.
(5) Budai, J., Bristowe, P. D. and Sass, S. L., Acta Metall. 31 (1983) 699.
(6) Stadelmann, P. A., Ultramicroscopy 21 (1987) 131.